Physical Science International Journal

Volume 28, Issue 4, Page 29-41, 2024; Article no.PSIJ.117178
ISSN: 2348-0130

The Influence of Anti-scatter Grid Usage for Knee Computerized Radiography

Luísa Vargas Cassol [a], Nataly Nogueira Favarin [a], Felipe de Bail [a], Edméia Lopes Ramai Buss [a], Laura Pizarro Trojahn Nogueira [a], Jéssica Fetzer da Costa Rosa [a] and Thiago Victorino Claus [b*]

[a] Universidade Franciscana (UFN), Santa Maria, RS, Brazil.
[b] Universidade Franciscana (UFN), Hospital Universitário de Santa Maria (HUSM), Santa Maria, RS, Brazil.

Authors' contributions

This work was carried out in collaboration among all authors. All authors read and approved the final manuscript.

Article Information

DOI: https://doi.org/10.9734/psij/2024/v28i4834

Open Peer Review History:
This journal follows the Advanced Open Peer Review policy. Identity of the Reviewers, Editor(s) and additional Reviewers, peer review comments, different versions of the manuscript, comments of the editors, etc are available here: https://www.sdiarticle5.com/review-history/117178

Original Research Article

Received: 04/05/2024
Accepted: 09/05/2024
Published: 13/05/2024

ABSTRACT

Aims: This experimental study investigated the effect of using an anti-scatter grid in computerized knee radiography (CR) on image quality (IQ) and patient surface radiation dose (Equivalent Surface Air Kerma – $K_{a,e}$), measured with an ionization chamber.
Place and Duration of Study: The experimental study was conducted between February 2024 and April 2024, in the radiodiagnosis laboratory belonging to the Medical Physics and Radiology Technology courses at the Franciscan University (UFN) in the city of Santa Maria, Rio Grande do Sul.

**Corresponding author: E-mail: clausrx@gmail.com;*

Methodology: Utilizing a semi-anatomical knee phantom to simulate clinical examination conditions, ten images were acquired, with five obtained using technique 1 (70 kV, 200mA, and 20mAs) and another five with technique 2 (70 kVp, 200mA, and 5 mAs), with and without an anti-scatter grid, respectively. The phantom images were digitized in a CR system and quantified using a publicly available automatic analyzer software based on histograms and regions of interest (ROI), defined by signal and noise. The obtained results were used to calculate the signal-to-noise ratio (SNR), contrast-to-noise ratio (CNR), and radiographic contrast (RC), considered IQ descriptors.
Results: As a selection criterion, the percentage deviation (D%) was chosen, considering technique 1 as the reference concerning technique 2. It was observed that technique 1 showed an SNR 1.20%, RC 3.86%, and $K_{a,e}$ 73.68% higher than technique 2; on the other hand, technique 2 indicated a CNR 4.76% higher compared to technique 1.
Conclusion: It is concluded that technique 2 without an anti-scatter grid may be preferable when considering the principle of optimization, where the dose is significantly reduced without a significant loss in IQ descriptors.

Keywords: Imaging radiodiagnosis; process optimization; radiography; knee; scattering radiation; signal-to-noise ratio.

1. INTRODUCTION

Computerized radiography (CR) of the knee is widely utilized as an accessible and economical method for the majority of the population, with an approximate incidence of 23.2% compared to other examinations [1]. During the radiographic examination, the acquisition of information regarding internal structure occurs through the interaction of X-rays, resulting in a primary component and another in radiation scatter [2].

Recent studies by Abela et al. [3] highlighted that the use of anti-scatter grids in knee examinations enhances image quality (IQ) by reducing radiation scatter. This may necessitate a considerable increase in radiation dose to the patient; however, they concluded that the use of anti-scatter grids may be omitted in certain knee thicknesses without significant loss in IQ.

Assessment of IQ can be conducted qualitatively and quantitatively. The former pertains to the visual perception of diagnostic features in the image, crucial for clinical diagnosis, while the latter involves physical measurements such as signal-to-noise ratio (SNR) and contrast-to-noise ratio (CNR), which are descriptors related to contrast, resolution, and noise in the image [4,5].

Radiation dose measurements are based on readings of Air Kerma, representing the energy deposited in the detector due to the interaction of the primary X-ray beam when adjusted for the distance between the X-ray focus and anatomy, namely, Entrance Skin Air Kerma ($K_{a,e}$) [6].

Excessive or insufficient X-ray exposures during radiographic examinations can result in images with little diagnostic value. The prevalence of interaction types, absorption, and/or scatter, is directly correlated with the energy of the involved radiations. In extremity examinations, such as knee examinations, the photoelectric effect predominates, while the decision regarding the use of anti-scatter grid is delicate due to anatomical location and patient biotype. Consequently, part of the incident photons on the tissue is absorbed, while the rest undergoes Compton scattering, responsible for X-ray scatter [7].

The implementation of the exposure index (EI) in digital systems (DS) has provided radiology professionals with an exposure parameter for the image receptor [8]. EI provides feedback on the radiation dose to the detector and the level of noise present in the image, if the reference value established by the DS manufacturer is not achieved [9]. Thus, the objective of this study was to evaluate the influence of anti-scatter grid use on IQ descriptors and radiation dose in anteroposterior (AP) knee examinations in CR systems.

2. MATERIALS AND METHODS

The study was conducted in the radiodiagnosis laboratory, affiliated with the courses of Medical Physics and Radiology Technology, as an integral part of ongoing investigations within the disciplines of Radiodiagnosis and Procedures III, which are part of the curriculum at Franciscana

University (UFN) in the city of Santa Maria, Rio Grande do Sul.

2.1 Image Acquisition and Radiation Dose Measurement

In this study, a radiographic system Intecal, model Radiologist's House (MAAF) (manufactured in July 2010, Brazil), and a digital image scanning system for CR from Carestream, model Vitaflex (manufactured in August 2018), were employed. The radiographic system was used for image acquisition and measurements of $K_{a,e}$, operating within a voltage range between 40 and 120 kV and an electric current between 100 and 630 mA, coupled with a high-frequency generator.

For image acquisition, a semi-anatomical phantom was used to simulate clinical examination conditions, with a thickness of 12 cm (Fig. 1). Ten images (radiographs) were obtained with the same cassette, five of them acquired with technique 1 using a grid with a 10:1 ratio (52 lines/cm) (Fig. 1A), and the other five with technique 2 without anti-scatter grid (Fig. 1B), maintaining a fixed distance from the source to the phantom surface of 1 meter.

A RADICAl dosimetric set, model 9015, was positioned and aligned with the sensitive area of the ionization chamber above the phantom, representing the patient's surface. A total of 10 exposures were performed as shown in Fig. 1C. For each group of five $K_{a,e}$ measurements for each technique, we calculated the mean value to reduce random error.

To digitize the images, a cassette of 24cm x 30cm, an imaging plate (IP) with a spatial resolution of 10 pixels/mm, and a resolution scale of 16 bits/pixel were used. This IP was processed in the reader of the CR system itself, and the resulting images were displayed on the workstation monitor. The electrical parameters, voltage (kV), and current-time product (mAs) selected on the control panel of the radiographic system are indicated in Table 1.

In our study, we kept the type of examination (knee), field size, beam energy (kV), and electrical current at 200mA constant for both techniques.

2.2 Image Quality

Quantitative evaluation of the images was facilitated by the public domain computational program ImageJ [10]. The program allowed for the generation of histograms for each image, displaying a graph in a new window. The histogram stands out as a useful tool for evaluating the intensity spectrum of the image matrix and quantifying the average signal and noise values. To quantify an overall analysis of IQ, the Signal-to-Noise Ratio (SNR).

$$SNR = \frac{Average\ of\ signal\ values}{Average\ of\ noise\ values} \quad (1)$$

(A) **(B)** **(C)**

Fig. 1 - Exposure geometry for image acquisition of the semi-anatomical phantom and radiation dose measurement

Table 1. Selected electrical parameters for each exposure technique

Electrical parameters	Technique 1 (With grid)	Technique 2 (Without grid)
Voltage (kV)	70	
mA.s	20	5

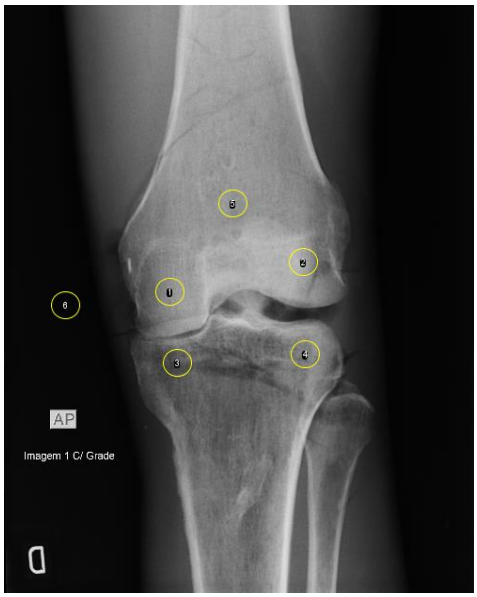

Fig. 2. Position of enumerated ROI/Anatomy. The first region was focused on the Medial Femoral Condyle (MFC), the second on the Lateral Femoral Condyle (LFC), the third on the Medial Tibial Condyle (MTC), the fourth on the Lateral Tibial Condyle (LTC), the fifth on the Femur, and the sixth on the Background ROI, representing the image background without anatomy

To identify regions of interest (ROI), the signal and noise of the captured images were selected in six specific areas for each examination/anatomy. These regions were defined in the image according to the following criteria: the first region was centered on the Medial Femoral Condyle (MFC), the second on the Lateral Femoral Condyle (LFC), the third on the Medial Tibial Condyle (MTC), the fourth on the Lateral Tibial Condyle (LTC), the fifth on the Femur, and the sixth on the Background ROI, representing the image background without anatomy. All regions were delineated circularly and had the same area (101,997 mm²), as shown in Fig. 2.

For each image, we evaluated the mean signal value (average of pixels) of each Region of Interest (ROI), as well as the corresponding noise (standard deviation). In pursuit of a comprehensive analysis of IQ, we calculated the Signal-to-Noise Ratio (SNR) and Contrast-to-Noise Ratio (CNR) for each ROI/Anatomy. The signal and noise values of each ROI were assessed following the methodology of Mraity et al. [11], to obtain a comprehensive analysis of IQ, according to Equations 2 and 3, respectively.

$$SNR = \frac{Signal\ Average\ ROIs\ 1; 2; 3; 4\ e\ 5}{Background\ Noise\ ROI\ 6} \quad (2)$$

$$CNR = \left| \frac{background\ signal\ (ROI\ 6) - signal\ values(ROI\ 1)}{Background\ Noise\ ROI\ 6} \right| \quad (3)$$

To evaluate the radiographic contrast (RC), the mean signal difference between ROI 1 (MFC) and ROI 6 (background) was chosen, as per Equation 4.

$$RC = (ROI\ 1) - (ROI\ 6) \quad (4)$$

The Signal-to-Noise Ratio (SNR) reflects the system's ability to detect signal intensity variations relative to background noise, indicating sensitivity to image resolution [4]. On the other hand, the Contrast-to-Noise Ratio (CNR) expresses the relationship between the intensity difference between two areas in the image and background noise, highlighting the ability to distinguish different levels of contrast in the image [12]. Radiographic Contrast (RC) represents the difference between signal intensities in two areas of interest in the image, offering a direct measure of contrast resolution [4].

As a criterion for selection due to the absence of established reference values to define the limits of IQ descriptors in radiodiagnosis, these values were considered those measured in the reference images acquired with technique 1 (with grid). To compare the acquired images with the

reference image, the use of percent deviation (D%) was chosen, as per Equation 5.

$$D(\%) = \left[\left(\frac{Technique\ 1\ (With\ grid)}{Technique\ 2\ (Without\ grid)}\right) - 1\right] \times 100 \quad (5)$$

3. RESULTS AND DISCUSSION

In Fig. 3, the 10 radiographs obtained from the phantom along with their respective histograms and signal and noise values for each ROI are presented. The signal values represent the average intensity of the radiographic signal, while the noise values represent the average variation of the signal around this mean value.

3.1 Dosimetry and Image Quality Results

In Table 2, the average values of $K_{a,e}$ readings in milligrays (mGy) obtained with the dosimetric set are represented, as well as the mean signal and noise values obtained from the histograms of each image and their respective Exposure Index (EI) values obtained with technique 1 (with grid) and technique 2 (without grid). With the IQ values, it was possible to calculate the Signal-to-Noise Ratio (SNR) using Equation 1 and perform the analysis of the results. In addition, the EI values were within and even below the maximum value set by the manufacturer, which considers the optimum values to be between 1800 and 2500.

In Table 2, it is observed that the average $K_{a,e}$ readings for exams with a grid are 2.500 mGy, whereas for exams without a grid, it is 0.658 mGy. This indicates that the $K_{a,e}$ readings for exams performed with a grid are consistently higher compared to exams performed without a grid (3.794 times higher). From the histogram results, it is evident that, on average, images obtained with an anti-scatter grid (technique 1) exhibit a relatively higher SNR (0.96) compared to images obtained without an anti-scatter grid (0.90). Tables 3 and 4 represent the mean signal and noise values obtained using ImageJ from the ROI/Anatomy for techniques 1 and 2, respectively.

In Tables 3 and 4, a variation in signal and noise values among different ROIs/anatomies is observed, concerning the images obtained with technique 1 and technique 2, respectively. In Table 3, ROI 2 (CFL) exhibits the highest signal and noise values compared to other ROIs, suggesting a high signal quality and a reasonable amount of noise. In Table 4, ROI 1 CFM (medial femoral condyle) shows relatively high signal and noise values compared to other ROIs, suggesting good signal quality and a reasonable amount of noise. However, in both techniques, ROI 6 (Background) presents the lowest signal and noise values, indicating weak signal and minimal noise, as expected for areas outside the region of interest. Table 5 represents the calculated values of SNR and CNR for the images obtained with and without the use of a grid, as well as the calculated mean values of the images and their respective percentage deviations in relation to Technique 1 (with grid).

In Table 5, it can be observed that Technique 1 has a relatively higher SNR compared to Technique 2, indicating better sensitivity to image resolution. However, the percentage difference is relatively small (-1.20%). Technique 2 exhibits a significantly higher CNR compared to Technique 1, indicating better differentiation between different levels of contrast in the image. The percentage difference is 4.76%, which is a considerable difference. The RC of Technique 1 is higher than that of Technique 2, indicating better contrast resolution. However, the percentage difference is relatively small (-3.86%). The radiation dose ($K_{a,e}$) in Technique 1 is significantly higher than in Technique 2, with a very large percentage difference of -73.68%. In Fig. 4, the values of the IQ descriptors (SNR, CNR, and RC) and $K_{a,e}$ (mGy) are graphically represented.

In Fig. 4, it is observed that choosing Technique 2 may minimally degrade the SNR and RC descriptors by 1.20% and 3.86%, respectively. However, there is an improvement in CNR by 4.76% compared to Technique 1. Nonetheless, a considerable difference in radiation dose between the two techniques is noted, without equal contribution to improving IQ with the use of anti-scatter grid in knee examinations. Understanding the image creation process and its relationship with contrast, noise, patient dose, and diagnostic performance enhances modern radiology practice [12].

In our study, histogram results suggest that choosing Technique 1 (with the use of anti-scatter grid) may improve SNR by 6.35% compared to Technique 2, indicating an advantage in the signal-to-noise ratio in knee radiographs. This is because radiation scatter generates grayscale areas in the image that do not directly correspond to the projected anatomy, leading to a significant contrast reduction in radiography, as highlighted by Bushberg & Boone [13].

Images obtained with anti-scatter grid

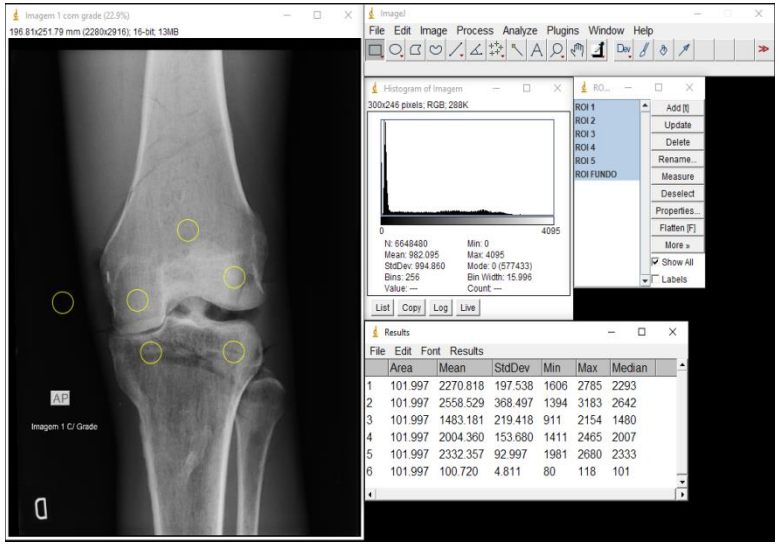

Images obtained without anti-scatter grid

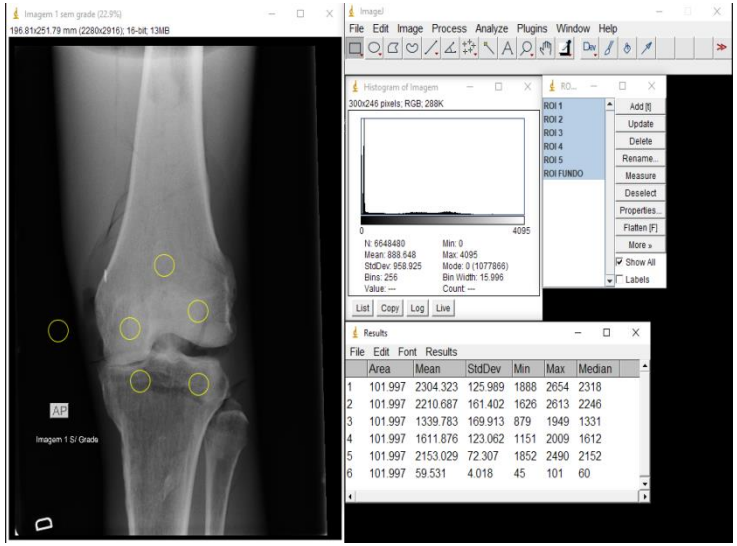

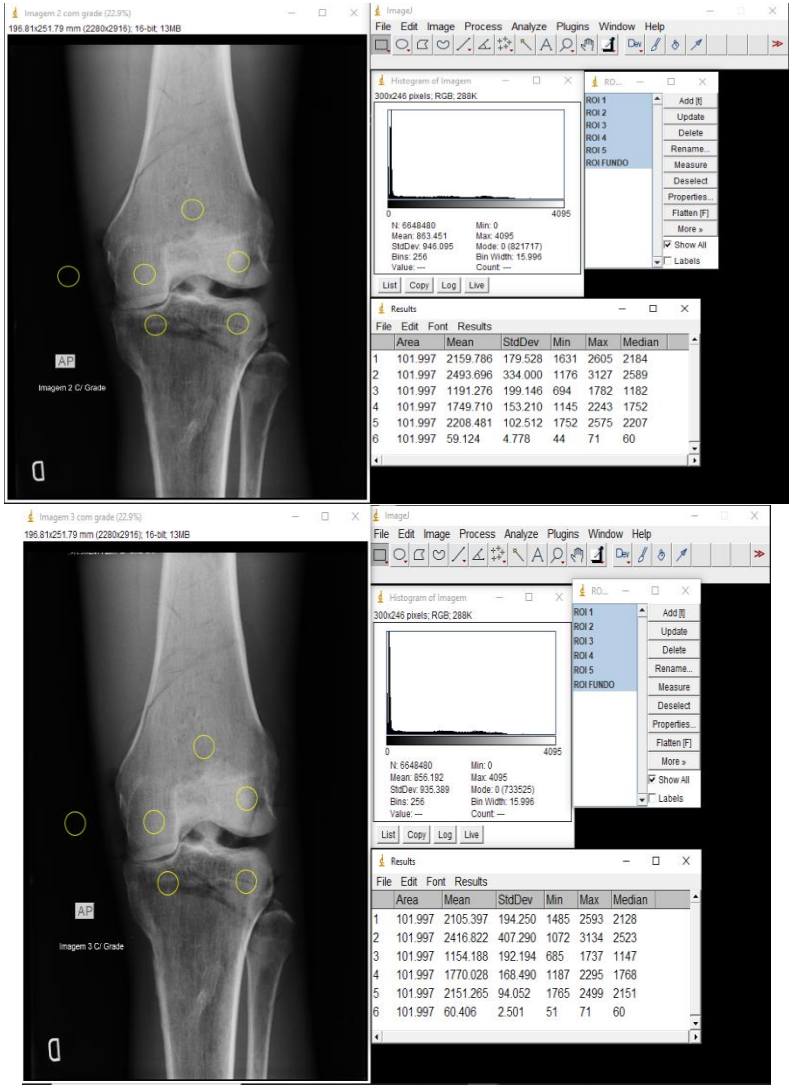
Imagem 2 com grade (22.9%)
196.81x251.79 mm (2280x2916); 16-bit; 13MB
AP
Imagem 2 C/ Grade
ImageJ
File Edit Image Process Analyze Plugins Window Help
Histogram of Imagem
300x246 pixels; RGB; 288K
N: 6648480
Mean: 863.451
StdDev: 946.095
Mode: 0 (821717)
Min: 0
Max: 4095
Bin Width: 15.996
Bins: 256
Value: ---
Count: ---
List Copy Log Live
RO...
ROI 1
ROI 2
ROI 3
ROI 4
ROI 5
ROI FUNDO
Add [t]
Update
Delete
Rename...
Measure
Deselect
Properties...
Flatten [F]
More »
Show All
Labels
Results
File Edit Font Results
Area Mean StdDev Min Max Median
1 101.997 2159.786 179.528 1631 2605 2184
2 101.997 2493.696 334.000 1176 3127 2589
3 101.997 1191.276 199.146 694 1782 1182
4 101.997 1749.710 153.210 1145 2243 1752
5 101.997 2208.481 102.512 1752 2575 2207
6 101.997 59.124 4.778 44 71 60

Imagem 3 com grade (22.9%)
196.81x251.79 mm (2280x2916); 16-bit; 13MB
AP
Imagem 3 C/ Grade
ImageJ
File Edit Image Process Analyze Plugins Window Help
Histogram of Imagem
300x246 pixels; RGB; 288K
N: 6648480
Mean: 856.192
StdDev: 935.389
Mode: 0 (733525)
Min: 0
Max: 4095
Bin Width: 15.996
Bins: 256
Value: ---
Count: ---
List Copy Log Live
RO...
ROI 1
ROI 2
ROI 3
ROI 4
ROI 5
ROI FUNDO
Add [t]
Update
Delete
Rename...
Measure
Deselect
Properties...
Flatten [F]
More »
Show All
Labels
Results
File Edit Font Results
Area Mean StdDev Min Max Median
1 101.997 2105.397 194.250 1485 2593 2128
2 101.997 2416.822 407.290 1072 3134 2523
3 101.997 1154.188 192.194 685 1737 1147
4 101.997 1770.028 168.490 1187 2295 1768
5 101.997 2151.265 94.052 1765 2499 2151
6 101.997 60.406 2.501 51 71 60

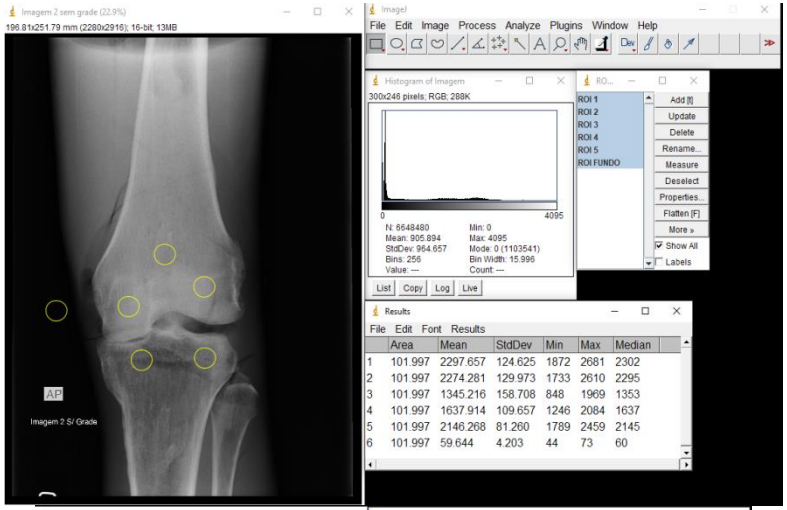
Imagem 2 sem grade (22.9%)
196.81x251.79 mm (2280x2916); 16-bit; 13MB
AP
Imagem 2 S/ Grade
ImageJ
File Edit Image Process Analyze Plugins Window Help
Histogram of Imagem
300x246 pixels; RGB; 288K
N: 6648480
Mean: 905.894
StdDev: 964.657
Mode: 0 (1103541)
Min: 0
Max: 4095
Bin Width: 15.996
Bins: 256
Value: ---
Count: ---
List Copy Log Live
RO...
ROI 1
ROI 2
ROI 3
ROI 4
ROI 5
ROI FUNDO
Add [t]
Update
Delete
Rename...
Measure
Deselect
Properties...
Flatten [F]
More »
Show All
Labels
Results
File Edit Font Results
Area Mean StdDev Min Max Median
1 101.997 2297.657 124.625 1872 2681 2302
2 101.997 2274.281 129.973 1733 2610 2295
3 101.997 1345.216 158.708 848 1969 1353
4 101.997 1637.914 109.657 1246 2084 1637
5 101.997 2146.268 81.260 1789 2459 2145
6 101.997 59.644 4.203 44 73 60

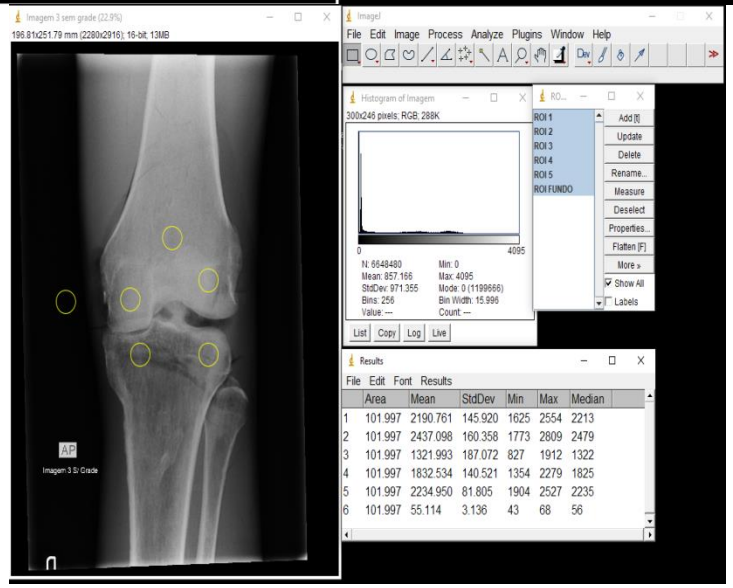
Imagem 3 sem grade (22.9%)
196.81x251.79 mm (2280x2916); 16-bit; 13MB
AP
Imagem 3 S/ Grade
ImageJ
File Edit Image Process Analyze Plugins Window Help
Histogram of Imagem
300x246 pixels; RGB; 288K
N: 6648480
Mean: 857.166
StdDev: 971.355
Mode: 0 (1199666)
Min: 0
Max: 4095
Bin Width: 15.996
Bins: 256
Value: ---
Count: ---
List Copy Log Live
RO...
ROI 1
ROI 2
ROI 3
ROI 4
ROI 5
ROI FUNDO
Add [t]
Update
Delete
Rename...
Measure
Deselect
Properties...
Flatten [F]
More »
Show All
Labels
Results
File Edit Font Results
Area Mean StdDev Min Max Median
1 101.997 2190.761 145.920 1625 2554 2213
2 101.997 2437.098 160.358 1773 2809 2479
3 101.997 1321.993 187.072 827 1912 1322
4 101.997 1832.534 140.521 1354 2279 1825
5 101.997 2234.950 81.805 1904 2527 2235
6 101.997 55.114 3.136 43 68 56

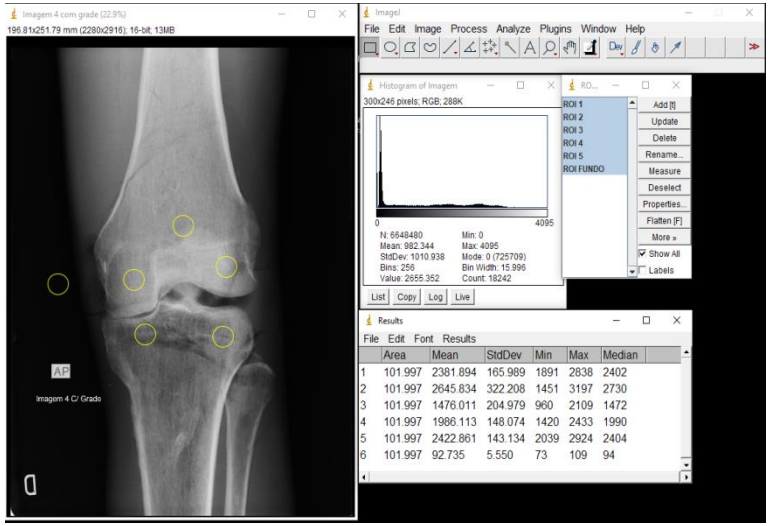

	Area	Mean	StdDev	Min	Max	Median
1	101.997	2381.894	165.989	1891	2838	2402
2	101.997	2645.834	322.208	1451	3197	2730
3	101.997	1476.011	204.979	960	2109	1472
4	101.997	1986.113	148.074	1420	2433	1990
5	101.997	2422.861	143.134	2039	2924	2404
6	101.997	92.735	5.550	73	109	94

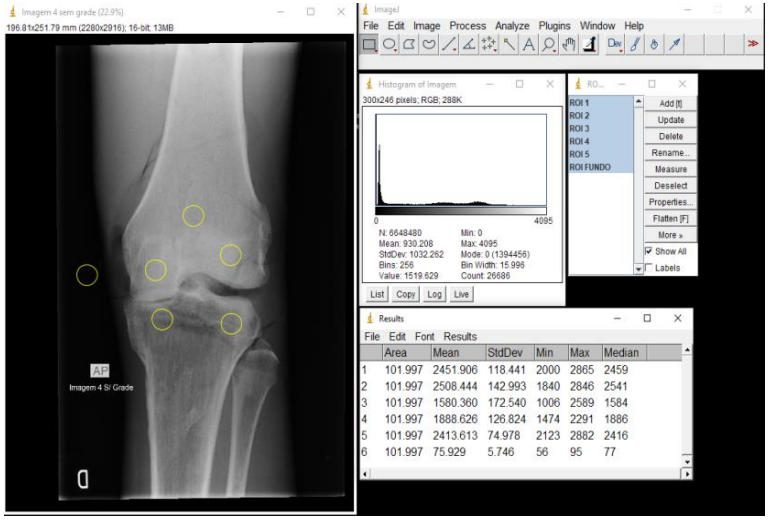

	Area	Mean	StdDev	Min	Max	Median
1	101.997	2451.906	118.441	2000	2865	2459
2	101.997	2508.444	142.993	1840	2846	2541
3	101.997	1580.360	172.540	1006	2589	1584
4	101.997	1888.626	126.824	1474	2291	1886
5	101.997	2413.613	74.978	2123	2882	2416
6	101.997	75.929	5.746	56	95	77

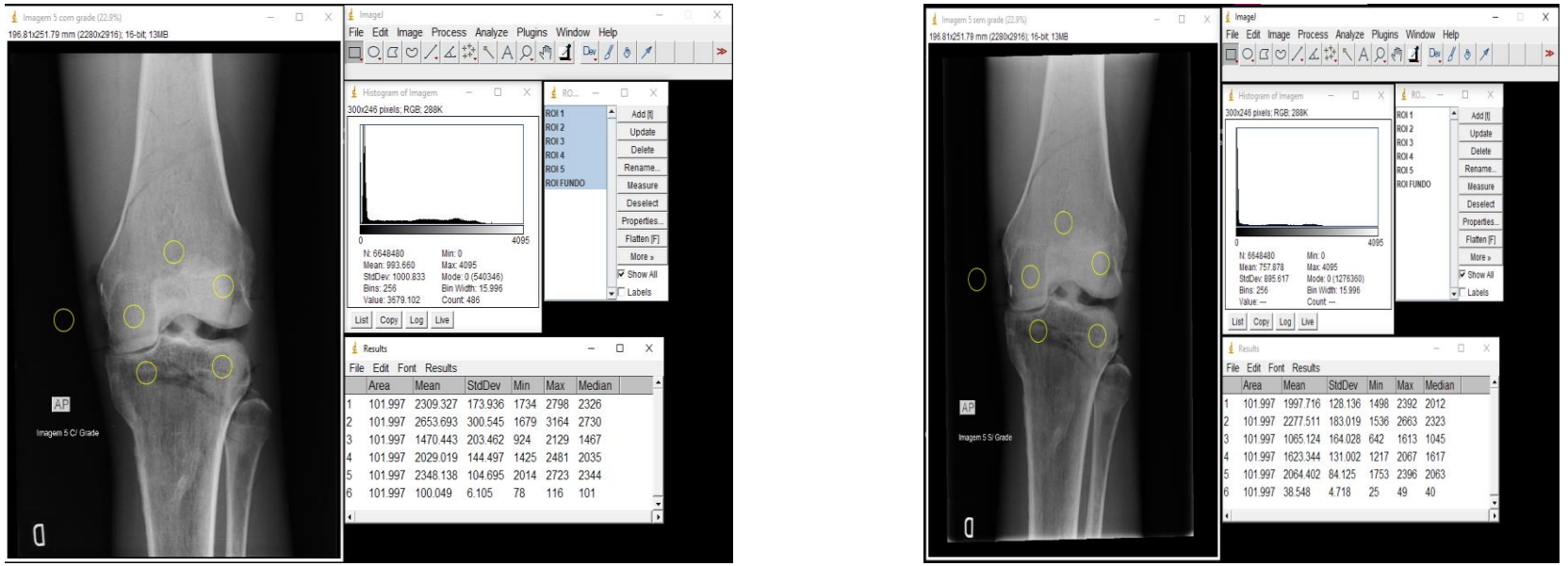

Fig. 3. Images and their respective Histograms and ROIs/Anatomy obtained with the Image J program

Table 2. Relationship of measured values of readings with techniques 1 and 2, as well as the mean value and standard deviation (SD)

Readings	Technique								
	1	2		1		2		1	2
	Radiation dose			IQ (Histograms)				Exposure Indicator	
	ESAK (mGy)		Image	Signal	Noise	Signal	Noise	EI	
Readings 1	2,492	0,660	Image 1	982,1	994,86	888,65	958,93	1871	2192
Readings 2	2,496	0,651	Image 2	863,45	946,1	905,89	964,66	2279	2132
Readings 3	2,507	0,658	Image 3	856,19	935,39	857,17	971,36	2276	2183
Readings 4	2,502	0,661	Image 4	982,34	1010,94	930,21	1032,26	1866	1944
Readings 5	2,502	0,660	Image 5	993,66	1000,83	757,88	895,62	1828	2371
Average	2,500	0,658	Average	935,55	977,62	867,96	964,56	2024	2164,4
SD	0,006	0,004	SNR	0,96		0,9		-	-
D%	-73,68%		D%	-6,25%				6,94%	

In Table 2, it is observed that the average $K_{a,e}$ readings for exams with a grid are 2.500 mGy, whereas for exams without a grid, it is 0.658 mGy. This indicates that the $K_{a,e}$ readings for exams performed with a grid are consistently higher compared to exams performed without a grid (3.794 times higher). From the histogram results, it is evident that, on average, images obtained with an anti-scatter grid (technique 1) exhibit a relatively higher SNR (0.96) compared to images obtained without an anti-scatter grid (0.90). Tables 3 and 4 represent the mean signal and noise values obtained using ImageJ from the ROI/Anatomy for techniques 1 and 2, respectively.

Table 3. Average Signal and Noise values obtained with technique 1 (with anti-scatter grid) for each ROI/Anatomy

		Image 1		Image 2		Image 3		Image 4		Image 5	
ROI	Anatomy	Signal	Noise	Signal	Noise	Signal	Noise	Signal	Noise	Signal	Noise
1	MFC	2270,8	197,5	2159,8	179,5	2105,4	194,3	2381,9	166,0	2309,3	173,9
2	LFC	2558,5	368,5	2493,7	334,0	2416,8	407,3	2645,9	322,2	2653,7	300,5
3	MTC	1483,2	219,4	1191,3	199,1	1154,2	192,2	1476,0	205,0	1470,4	203,5
4	LTC	2004,4	153,7	1749,7	153,2	1770,0	168,5	1986,1	148,1	2029,0	144,5
5	Femur	2332,4	93,0	2208,5	102,5	2151,3	94,1	2422,9	143,1	2348,1	104,7
6	Background	100,7	4,8	59,1	4,8	60,4	2,5	92,7	5,6	100,0	6,1

Table 4. Average Signal and Noise values obtained with technique 2 (without anti-scatter grid) for each ROI/Anatomy

		Image 1		Image 2		Image 3		Image 4		Image 5	
ROI	**Anatomy**	**Signal**	**Noise**	**Signal**	**Noise**	**Signal**	**Noise**	**Signal**	**Noise**	**Signal**	**Noise**
1	MFC	2304,3	126,0	2297,7	124,6	2190,8	145,9	2451,9	118,4	1997,7	128,1
2	LFC	2210,7	161,4	2274,3	130,0	2437,1	160,4	2508,4	143,0	2277,5	173,0
3	MTC	1339,8	169,9	1345,2	158,7	1322,0	187,1	1580,4	172,5	1065,1	164,0
4	LTC	1611,9	123,1	1637,9	109,7	1832,5	140,5	1888,6	126,8	1623,3	131,0
5	Femur	2153,0	72,3	2146,3	81,3	2235,0	81,8	2413,6	75,0	2064,4	84,1
6	Background	59,5	4,0	59,6	4,2	55,1	3,1	75,9	5,7	38,5	4,7

In Tables 3 and 4, a variation in signal and noise values among different ROIs/anatomies is observed, concerning the images obtained with technique 1 and technique 2, respectively. In Table 3, ROI 2 (CFL) exhibits the highest signal and noise values compared to other ROIs, suggesting a high signal quality and a reasonable amount of noise. In Table 4, ROI 1 CFM (medial femoral condyle) shows relatively high signal and noise values compared to other ROIs, suggesting good signal quality and a reasonable amount of noise. However, in both techniques, ROI 6 (Background) presents the lowest signal and noise values, indicating weak signal and minimal noise, as expected for areas outside the region of interest. Table 5 represents the calculated values of SNR and CNR for the images obtained with and without the use of a grid, as well as the calculated mean values of the images and their respective percentage deviations in relation to Technique 1 (with grid).

Table 5. Image quality descriptors for techniques 1 and 2

	Technique 1 (with grid).			Technique 2 (Without grid)		
	SNR	**CNR**	**RC**	**SNR**	**CNR**	**RC**
Image 1	442,7	451,1	2304,3	478,8	558,7	2170,1
Image 2	410,3	439,7	2297,7	461,6	532,5	2100,7
Image 3	767,5	817,7	2190,8	638,9	681,0	2045
Image 4	393,3	412,5	2451,9	377,4	413,5	2289,2
Image 5	354,2	361,9	1997,7	382,7	415,3	2209,3
Average	473,6	496,5	2248,5	467,9	520,2	2161,8
D% SNR	-1,20%					
D% CNR	4,76%					
D% RC	-3,86%					

In Table 5, it can be observed that Technique 1 has a relatively higher SNR compared to Technique 2, indicating better sensitivity to image resolution. However, the percentage difference is relatively small (-1.20%). Technique 2 exhibits a significantly higher CNR compared to Technique 1, indicating better differentiation between different levels of contrast in the image. The percentage difference is 4.76%, which is a considerable difference. The RC of Technique 1 is higher than that of Technique 2, indicating better contrast resolution. However, the percentage difference is relatively small (-3.86%). The radiation dose ($K_{a,e}$) in Technique 1 is significantly higher than in Technique 2, with a very large percentage difference of -73.68%. In Figure 4, the values of the IQ descriptors (SNR, CNR, and RC) and $K_{a,e}$ (mGy) are graphically represented.

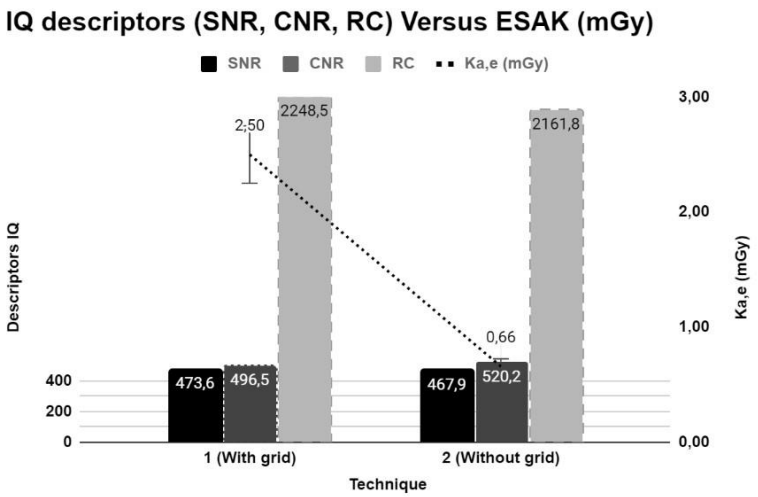

Fig. 4. Comparison between IQ Descriptors Versus Radiation Dose ($K_{a,e}$)

However, when comparing the calculated mean values of signal-to-noise ratio (SNR), contrast-to-noise ratio (CNR), and radiographic contrast (RC) concerning the values obtained from the ROIs, minimal differences between the two techniques are revealed: Technique 1 showed an SNR 1.20%, RC 3.86% higher than Technique 2. However, a significant difference in $K_{a,e}$, 73.68% higher than Technique 2, while Technique 2 indicated an CNR 4.76% higher than Technique 1.

Studies by Huda & Abrahams [12] concluded in their studies that CNR can be seen as a relative descriptor of the visibility of a specific lesion, suggesting that increasing contrast, reducing noise, or adopting a balanced combination of these two aspects can enhance its visualization. Other studies by Tompe & Sargar [5] found that contrast remains constant in these images, regardless of radiation exposure, which can be used to optimize the process and result in additional radiation dose reduction to the patient. Studies by Abela et al. [3] corroborate with our findings, demonstrating a significant reduction in radiation dose and an improvement in IQ without the use of anti-scatter grid for a thickness of 12 cm.

This analysis suggests that optimizing diagnostic accuracy through excessive exposure may not be the most appropriate strategy, as improving visualization of anatomical structures of interest may not be achieved solely through additional dose increments. Additionally, the electrical parameters of the exposure technique, such as voltage (kV) and current-time product (mA.s), directly influence the workload and lifespan of the radiographic tube, with the use of lower loads (Technique 2) possibly associated with a longer lifespan of the radiographic tube.

4. CONCLUSION

The results indicate that although Technique 1 with anti-scatter grid may improve the signal-to-noise ratio (SNR), it comes with a significant cost in terms of radiation dose ($K_{a,e}$) and image quality (IQ). While Technique 2 demonstrated superior contrast resolution capability and a longer lifespan of the radiographic tube, suggesting that a balanced approach, considering technical and clinical factors, is essential to optimize IQ and minimize $K_{a,e}$ for patients during clinical practice.

ACKNOWLEDGEMENTS

The intellectual incentive of the professors of the Undergraduate Medical Physics and Radiology courses at the Franciscan University (UFN).

COMPETING INTERESTS

Authors have declared that no competing interests exist.

REFERENCES

1. Da rocha DGVB, Marcelino LG. Knee trauma approach and treatment: A systematic review. Brazilian Journal of Development. 2022;8(5):33902-33912.

2. Henner A, Ilves S, Yrjänheikki T. Demonstrating the scattering of radiation in radiographic imaging. European Congress of Radiology-ECR 2015; 2015, March.
3. Abela N, Couto JG, Zarb F, Mizzi D. Evaluating the use of anti-scatter grids in adult knee radiography. Radiography. 2022;28(3):663-667.
4. Moore CS, Wood TJ, Jones S, Saunderson JR, Beavis AW. A practical method to calibrate and optimise automatic exposure control devices for computed radiography (CR) and digital radiography (DR) imaging systems using the signal-to-noise ratio (SNR) metric. Biomedical Physics & Engineering Express. 2019; 5(3):035027.
5. Tompe A, Sargar K. X-ray image quality assurance; 2020.
6. Metaxas VI, Messaris GA, Lekatou AN, Petsas TG e Panayiotakis GS. Patient doses in common diagnostic X-ray examinations. 2019;184(1):12-27.
7. Dimenstein R, Ghilardi Netto T. Physical and technological bases applied to x-rays. In Physical and Technological Bases Applied to X-rays. 2005;90-90.
8. Seeram E, Davidson R, Bushong S, Swan H. Optimizing the exposure indicator as a dose management strategy in computed radiography. Radiologic Technology. 2016; 87(4):380-391.
9. Braga LF, Pimentel RB, Dias TS, Assunção MF, Salido FS, Neves RF, Freitas MB. Methodology for analysis and interpretation of exposure indicators (EI) and their deviations (DI) in computerized radiology. Brazilian Journal of Medical Physics. 2019;13(3):33-37.
10. Wayne R. Software for image processing and analysis. USA: National Institute of Mental Health, java; 2024. Available:http://rsbweb.nih.gov/ij/download.html
11. Mraity HA, England A, Cassidy S, Eachus P, Dominguez A, Hogg P. Development and validation of a visual grading scale for assessing image quality of AP pelvis radiographic images. The British Journal of Radiology. 2016;89 (1061): 20150430.
12. Huda W, Abrahams RB. Radiographic techniques, contrast, and noise in x-ray imaging. American Journal of Roentgenology. 2015;204(2):W126-W131.
13. Bushberg JT, Boone JM. The essential physics of medical imaging. Lippincott Williams & Wilkins; 2011.

Peer-review history:
The peer review history for this paper can be accessed here:
https://www.sdiarticle5.com/review-history/117178